SHAPE OPTIMIZATION METHOD FOR DESIGNING INTERFACE SHAPES OF COMPOSITE CLAD STRUCTURES

M. Shimoda[1*], S. Motora[2], H. Ohtani[3]

[1]*Department of Advanced Science and Technology, Toyota Technological Institute, 2-12-1, Hisakata, Tenpaku-ku, Nagoya, Aichi 468-8511, Japan*
[2]*Engineering System Service Division, Toshiba I. S. Corporation, 1-1-43 Shibaura, Minato Ward, Tokyo105-0023, Japan*
[3]*Graduate School of Toyota Technological Institute, 2-12-1, Hisakata, Tenpaku-ku, Nagoya, Aichi 468-8511, Japan*
**shimoda@toyota-ti.ac.jp*

Keywords: shape optimization, optimum design, interface shape, clad material

Abstract
This paper proposes a shape optimization method for designing the interface shapes of composite clad structures consisting of two different materials. The outer boundaries and the interface boundaries are considered as the design boundaries for determining the shape of the clad structure. The compliance is minimized under the volume constraints of the two materials. The shape gradient function for this type of problem is derived using the material derivative and adjoint methods and is applied to the traction method, a gradient method in a Hilbert space. With this method, the optimal outer and interface boundary shapes can be determined with mesh regularity and without requiring shape design parameterization, while minimizing compliance. The validity of the proposed method for the interface design of clad structures was verified on the basis of calculated results.

1 Introduction
Clad materials fabricated by bonding two or more different materials are types of composite materials that are extensively used in many industrial products. The most notable feature of clad materials is that new properties are obtained by combining the different constituent materials. The combinations of materials, thicknesses and widths often become design variables in the design of clad materials. It is expected that even more new properties can be obtained by adding the interface shape to the design variables in the design of clad structures, which is the motivation for this research. This idea can also be applied to other composite structures with thick layers such as fiber-reinforced plastic and metal-plastic composites.
Interface shape optimization problems can be defined by combining two or more different media or materials such as a structure-fluid problem [1]-[3]. In this paper, a linear elastic body of different materials is treated. In studies of interface shape optimization problems of elastic bodies to date, Haug et al. derived the shape sensitivity in their monograph [4]. Choi et al. presented an application to implant design in dentistry [5]. In contrast, in our previous works, we have developed the traction method, and applied it to various shape design problems of 2D and 3D continua, involving plate and shell structures [6]-[8]. The traction method, a gradient method in a Hilbert space, was proposed as a solution to domain optimization problems by Azegami [9]. With this method an arbitrary smooth boundary shape is obtained without any

shape parameterization. In this paper, the traction method is applied to the interface shape optimization problem of composite clad structures consisting of two dissimilar materials. The interface and outer boundaries are treated as the shape design boundaries to be determined. A stiffness design problem is defined by using compliance as the objective functional and the two material volumes as the constraint conditions. A distributed-parameter shape optimization problem is formulated, and the shape gradient function, i.e., a shape sensitivity function, is derived. The shape gradient function is applied to the design boundaries as a pseudo-traction force to vary the shape. This analysis also serves to smooth the boundaries, since it is important for node-based shape optimization methods to resolve the jagged boundary problem. In the following chapters, the domain variation, the formulation of the problem, and the optimization method will be described. Then, calculated results will be presented.

2 Domain variation for shape optimization

A technique for representing domain variation using the speed method will be introduced briefly before formulating the shape optimization problem. A detailed explanation of this technique may be found in references [4], [10] and [11].

As shown in Fig. 1, it is assumed that a linear elastic body having an initial global domain of $\Omega \subset \mathbb{R}^3$ and its boundary $\Gamma \equiv \partial\Omega$ with two different materials A and B undergoes variation (i.e., the design velocity field) $\boldsymbol{V}$ such that its domain and boundary become Ω_s and Γ_s. Sub-domains and their boundaries with material A are defined as Ω_A, Γ_A, and with B as Ω_B, Γ_B, respectively. The interface between Ω_A and Ω_B are defined as $\Gamma_{AB} \equiv \Gamma_A \bigcap \Gamma_B$. The notation $\mathbb{R}$ indicates a set of positive real numbers. The domain variation can be expressed by a one-to-one mapping $T_S(\boldsymbol{X}) : X \in \Omega \mapsto x \in \Omega_S$, $0 \le s < \varepsilon$. The notations s and ε indicate the iteration history of domain variation and a small positive number, respectively. Assuming a constraint is acting on the variation in the domain $\Theta \subset \Omega$, the infinitesimal variation of the domain can be given by

$$T_{s+\Delta s}(\boldsymbol{X}) = T_s(\boldsymbol{X}) + \Delta s \boldsymbol{V} \tag{1}$$

where the design velocity field $\boldsymbol{V}$ is given as a derivative of $T_s(\boldsymbol{X})$ with respect to s and can be defined as a piecewise continuous function as

$$\boldsymbol{V}(\boldsymbol{x}) = \frac{\partial T_s}{\partial s}(T_s^{-1}(\boldsymbol{x})), \quad \boldsymbol{x} \in \Omega_s, \qquad \boldsymbol{V} \in C_\Theta = \{\boldsymbol{V} \in C^1(\Omega; \mathbb{R}^3) \mid \boldsymbol{V} = \boldsymbol{0} \text{ in } \Theta\} \tag{2}$$

where C_Θ is the suitably smooth function space that satisfies the constraints of domain variation. The optimal design velocity field $\boldsymbol{V}$ is determined by the traction method which will be explained later.

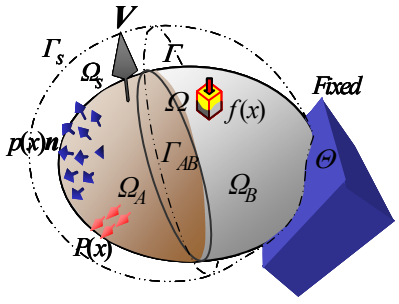

Figure 1. Domain variation of Continuum consist of two materials.

3 Formulation of shape optimization problem of solid structure

Here we will solve the non-parametric shape optimization problem for the rigidity design of a clad structure with linear elastic materials *A* and *B*. Consider that body forces per unit volume $\boldsymbol{f}(\boldsymbol{x})$, surface forces per unit area $\boldsymbol{P}(\boldsymbol{x})$ and pressure $p(\boldsymbol{x})\boldsymbol{n}$ act on Ω, Γ_1 and Γ_2, respectively. Letting $l(\boldsymbol{v})$ denote compliance as an index of rigidity, the compliance minimization problem subject to the constraints of M, M_A and the state equation can be formulated as shown below.

$$\text{Find} \quad \Omega_s \text{ and } \Gamma_{AB_s}, \tag{3}$$

$$\text{that minimizes} \quad l(\boldsymbol{v}), \tag{4}$$

$$\text{subject to} \quad M(=\int_{\Omega_s} d\Omega) = \hat{M}, \quad M_A(=\int_{\Omega_{As}} d\Omega) = \hat{M}_A, \tag{5}$$

$$a_A(\boldsymbol{v},\boldsymbol{w}) - h_A(\boldsymbol{v},\boldsymbol{w}) + a_B(\boldsymbol{v},\boldsymbol{w}) - h_B(\boldsymbol{v},\boldsymbol{w}) = l(\boldsymbol{w}), \quad \forall \boldsymbol{w} \in U, \tag{6}$$

where M and M_A denote the total volume and the volume with material *A*, respectively. The notation $\hat{(\ )}$ indicates the constraint value. The bilinear forms $a_m(\boldsymbol{v},\boldsymbol{w})$ and $h_m(\boldsymbol{v},\boldsymbol{w})$ (m=*A,B*) and the linear form $l(\boldsymbol{w})$ are defined as

$$a_m(\boldsymbol{v},\boldsymbol{w}) = \int_{\Omega_m} \sigma_{ij}^m(\boldsymbol{v})\varepsilon_{ij}^m(\boldsymbol{w}) d\Omega, \tag{7}$$

$$h_m(\boldsymbol{v},\boldsymbol{w}) = \int_{\Omega_m} \sigma_{i,j}^m n_j^m w_i d\Omega \tag{8}$$

$$l(\boldsymbol{w}) = \int_{\Omega} f_i w_i d\Omega + \int_{\Gamma_1} P_i w_i d\Gamma + \int_{\Gamma_2} p(\boldsymbol{x}) n_i w_i d\Gamma, \tag{9}$$

$$\varepsilon_{ij}^m(\boldsymbol{v}) = \frac{1}{2}(v_{i,j}^m + v_{j,i}^m), \quad \sigma_{ij}^m(\boldsymbol{v}) = C_{ijkl}^m \varepsilon_{i,j}^m(\boldsymbol{v}) \tag{10)(11}$$

where $\boldsymbol{v}^m$, $\boldsymbol{w}$ and C_{ijkl}^m are the displacement vectors, the variational displacement vector and the elastic coefficients, respectively, and U denotes the kinematically admissible displacement space that satisfies the Dirichlet condition. The tensor notation employed in this paper uses Einstein's summation convention and a partial differential notation $(\cdot)_{,i} = \partial(\cdot)/\partial x_i$.

Letting $\boldsymbol{w}$ and Λ, Λ_A denote the Lagrange multipliers for the constraints of the state equation, M and M_A, respectively, the Lagrangian functional L for this problem can be expressed as

$$L(\Omega,\boldsymbol{v},\boldsymbol{w},\Lambda) = l(\boldsymbol{v}) - a_A(\boldsymbol{v},\boldsymbol{w}) + h_A(\boldsymbol{v},\boldsymbol{w}) - a_B(\boldsymbol{v},\boldsymbol{w}) + h_B(\boldsymbol{v},\boldsymbol{w}) + l(\boldsymbol{w}) + \Lambda_A(M_A - \hat{M}_A) + \Lambda(M - \hat{M}) \tag{12}$$

Assuming that the Dirichlet boundaries are not varied with respect to *s*, the material derivative $\dot{L}$ with respect to the domain variation of the Lagrangian functional L is expressed using the design velocity field $\boldsymbol{V}$ as follows:

$$\dot{L} = l(\boldsymbol{v}') - a_A(\boldsymbol{v}',\boldsymbol{w}) - a_A(\boldsymbol{v},\boldsymbol{w}') + h_A(\boldsymbol{v}',\boldsymbol{w}) + h_A(\boldsymbol{v},\boldsymbol{w}') - a_B(\boldsymbol{v}',\boldsymbol{w}) - a_B(\boldsymbol{v},\boldsymbol{w}') + h_B(\boldsymbol{v}',\boldsymbol{w}) + h_B(\boldsymbol{v},\boldsymbol{w}') + l(\boldsymbol{w}') + \dot{\Lambda}_A(M_A - \hat{M}_A) + \dot{\Lambda}(M - \hat{M}) + \langle G\boldsymbol{n}, \boldsymbol{V} \rangle \tag{13}$$

where

$$\begin{aligned}\langle G\boldsymbol{n},\boldsymbol{V}\rangle &= \int_\Omega f_i' w_i d\Omega + \int_\Gamma (f_i w_i + \Lambda) V_n d\Gamma + \int_{\Gamma_A} \Lambda_A V_n^A d\Gamma - \int_{\Gamma_A\setminus\Gamma_{AB}} \sigma_{ij}^A(\boldsymbol{v})\varepsilon_{ij}^A(\boldsymbol{w}) V_n^A d\Gamma \\ &-\int_{\Gamma_B\setminus\Gamma_{AB}} \sigma_{ij}^B(\boldsymbol{v})\varepsilon_{ij}^B(\boldsymbol{w}) V_n^B d\Gamma + \int_{\Gamma_{AB}} [\{-\sigma_{ij}^A(\boldsymbol{v})\varepsilon_{ij}^A(\boldsymbol{w}) + (\sigma_{ij}^A(\boldsymbol{v})n_j^A w_i)_{,m} n_m^A + (\sigma_{ij}^A(\boldsymbol{v})n_j^A w_i)\kappa^A\} V_n^A \\ &+\{-\sigma_{ij}^B(\boldsymbol{v})\varepsilon_{ij}^B(\boldsymbol{w}) + (\sigma_{ij}^B(\boldsymbol{v})n_j^B w_i)_{,m} n_m^B + (\sigma_{ij}^B(\boldsymbol{v})n_j^B w_i)\kappa^B\} V_n^B] d\Gamma \\ &+\int_{\Gamma_1} \{P_i' w_i + (P_{i,j} n_j w_i + P_i w_{i,j} n_j + \kappa P_i w_i) V_n\} d\Gamma + \int_{\Gamma_2} \{p' w_i n_i + \mathrm{div}(p w_i) V_n\} d\Gamma \end{aligned} \quad (14)$$

where $V_n = n_i V_i$, $\boldsymbol{V}_n^m = n_i^m V_i^m(\boldsymbol{x})$. The vector $\boldsymbol{n}$ is an outward unit normal vector to the boundary. The notation $(\cdot)'$ indicates a shape derivative and has a relation of $\dot{(\cdot)} = (\cdot)' + (\cdot)_{,i} V_i$ [4] [10]. The notation κ expresses twice the mean curvature of Γ in $\mathbb{R}^3$. Considering the following relationship

$$\boldsymbol{n}^A = -\boldsymbol{n}^B, \quad \kappa^A = -\kappa^B, \quad \sigma_{ij}^A n_j^A = -\sigma_{ij}^B n_j^B, \quad (15)(16)(17)$$

and assuming that $\boldsymbol{f}$, $\boldsymbol{P}$ and p are not varied with respect to s within the space (i.e., $f'(\boldsymbol{x}) = P'(\boldsymbol{x}) = p'(\boldsymbol{x}) = 0$), $\langle G\boldsymbol{n},\boldsymbol{V}\rangle$ can be expressed as the dot product of the shape gradient function (i.e., shape sensitivity function) $\boldsymbol{G}(\equiv G\boldsymbol{n})$ and the design velocity field $\boldsymbol{V}$ as shown in the following equations.

$$\begin{aligned}\langle G\boldsymbol{n},\boldsymbol{V}\rangle &= \int_\Gamma G V_n d\Gamma + \int_{\Gamma_A\setminus\Gamma_{AB}} G_A V_n^A d\Gamma + \int_{\Gamma_B\setminus\Gamma_{AB}} G_B V_n^B d\Gamma + \int_{\Gamma_{AB}} G_{AB} V_n^A d\Gamma \\ &+\int_{\Gamma_1} G_1 V_n d\Gamma + \int_{\Gamma_2} G_2 V_n d\Gamma + \int_{\Gamma_A} G_{0A} V_n^A d\Gamma, \end{aligned} \quad (18)$$

$$G = f_i w_i + \Lambda, \quad G_A = -\sigma_{ij}^A(\boldsymbol{v})\varepsilon_{ij}^A(\boldsymbol{w}), \quad G_B = -\sigma_{ij}^B(\boldsymbol{v})\varepsilon_{ij}^B(\boldsymbol{w}), \quad (19)(20)(21)$$

$$G_{AB} = -\{\sigma_{ij}^A(\boldsymbol{v})\varepsilon_{ij}^A(\boldsymbol{w}) - \sigma_{ij}^B(\boldsymbol{v})\varepsilon_{ij}^B(\boldsymbol{w})\} + \sigma_{ij}^A(\boldsymbol{v}) n_j^A \{\varepsilon_{im}^A(\boldsymbol{w}) - \varepsilon_{im}^B(\boldsymbol{w})\} n_m^A \quad (22)$$

$$G_1 = P_{i,j} n_j w_i + P_i w_{i,j} n_j + \kappa P_i w_i, \quad G_2 = \mathrm{div}(p w_i), \quad G_{0A} = \Lambda_A \quad (23)(24)(25)$$

The optimality conditions of this functional L are expressed as shown below.

$$a_A(\boldsymbol{v},\boldsymbol{w}') - h_A(\boldsymbol{v},\boldsymbol{w}') + a_B(\boldsymbol{v},\boldsymbol{w}') - h_B(\boldsymbol{v},\boldsymbol{w}') = l(\boldsymbol{w}'), \quad \forall \boldsymbol{w}' \in U, \quad (26)$$

$$a_A(\boldsymbol{v}',\boldsymbol{w}) - h_A(\boldsymbol{v}',\boldsymbol{w}) + a_B(\boldsymbol{v}',\boldsymbol{w}) - h_B(\boldsymbol{v}',\boldsymbol{w}) = l(\boldsymbol{v}'), \quad \forall \boldsymbol{v}' \in U, \quad (27)$$

$$M_A - \hat{M}_A = 0, \quad M - \hat{M} = 0, \quad (28)(29)$$

where Eq. (26) is the governing equation of $\boldsymbol{v}$ which coincides with the state equation, Eq. (6), and Eq. (27) is the governing equation of $\boldsymbol{w}$, which is called the adjoint equation. The Lagrange multipliers Λ and Λ_A are determined so as to satisfy the volume constraints of Eqs. (28) and (29). Further, the relationship of Eq. (26) and Eq. (27) yields the self-adjoint relationship $\boldsymbol{v}=\boldsymbol{w}$.

By substituting $\boldsymbol{v}$ (or $\boldsymbol{w}$) into Eq. (13), the material derivative $\dot{L}$ can be given by the following equation.

$$\begin{aligned}\dot{L} &= \langle G\boldsymbol{n},\boldsymbol{V}\rangle \equiv \int_\Gamma G\boldsymbol{n}\cdot\boldsymbol{V} d\Gamma \left(\equiv \int_\Gamma \boldsymbol{G}\cdot\boldsymbol{V} d\Gamma\right) \\ &= \int_\Gamma G V_n d\Gamma + \int_{\Gamma_A\setminus\Gamma_{AB}} G_A V_n^A d\Gamma + \int_{\Gamma_B\setminus\Gamma_{AB}} G_B V_n^B d\Gamma + \int_{\Gamma_{AB}} G_{AB} V_n^A d\Gamma \end{aligned}$$

$$+\int_{\Gamma_1} G_1 V_n d\Gamma + \int_{\Gamma_2} G_2 V_n d\Gamma + \int_{\Gamma_A} G_{0A} V_n^A d\Gamma \,, \qquad (30)$$

The derived shape gradient function is applied to the traction method to determine the optimal design velocity $\boldsymbol{V}$.

4 Traction method

The traction method is a gradient method in a Hilbert space [11]. With the traction method, the negative shape gradient function $-\boldsymbol{G}$ is applied in the normal direction to the design boundary as an external distributed traction force to vary the shape with an elastic support (referred to here as the Robin-type traction method) or without an elastic support (referred to here as the Neumann-type traction method). A shape design constraint is applied as the Dirichlet condition. The elastic tensor is used as the positive definite tensor needed in the gradient method. We call this process the velocity analysis, or a pseudo-elastic analysis. The resultant displacement field (i.e., design velocity field) $\Delta s\boldsymbol{V}$ represents the amount of domain variation added to the original shape to update it. This shape updating decreases the objective functional.

The governing equation of the velocity analysis with the Neumann condition is given as Eq. (31) and with the Robin condition (α : a distributed spring constant per unit area) as Eq. (32) [12]. The Robin type is used in this work.

$$a(\boldsymbol{V},\boldsymbol{w}) = -\langle G\boldsymbol{n},\boldsymbol{w}\rangle, \quad \forall \boldsymbol{w} \in C_\Theta \,. \qquad (31)$$

$$a(\boldsymbol{V},\boldsymbol{w}) + \alpha\langle(\boldsymbol{V}\cdot\boldsymbol{n})\boldsymbol{n},\boldsymbol{w}\rangle = -\langle G\boldsymbol{n},\boldsymbol{w}\rangle, \quad \forall \boldsymbol{w} \in C_\Theta \,, \qquad (32)$$

where

$$a(\boldsymbol{V},\boldsymbol{w}) = \int_\Omega \sigma_{ij}(\boldsymbol{V})\varepsilon_{ij}(\boldsymbol{w})d\Omega \,. \qquad (33)$$

Equations (31) and (32) can be solved by a standard finite element analysis.

By repeating the stiffness analysis and the adjoint analysis (omitted in this work) for obtaining the shape gradient function, the velocity analysis and the updating of the shape by $\Delta s\boldsymbol{V}$, the objective functional is minimized, resulting in the smooth optimum shape.

Other features of this method are summarized as follows: (1) it is not necessary to parameterize the shape because all nodes on the design domain can be moved as the design variable (theoretically infinite degrees of freedom) and the shape sensitivity is efficiently calculated by the adjoint method, (2) it is not necessary to refine the mesh because the entire domain can be varied by the distributed force, (3) it assures smooth boundary shapes without any jagged shape problem because the elastic tensor serves as a smoother, and (4) it can be easily implemented in combination with a commercial FEM code because the shape gradient function is derived without differentiating the stiffness matrix with respect to the design variables. More details of the traction method involving the verification of smoothness are given in references [11] and [13].

5 Calculated results

To confirm the validity of the proposed method, it was applied to three design problems. In all problems, it was assumed that the surface forces applied were not varied with respect to *s*.

5.1 Cantilever beam problem with two layers

The first one is a simple solid cantilever beam problem with two different material layers *A* and *B*. The initial shape and the boundary conditions for this problem are shown in Fig. 2. The

boundary condition for the stiffness analysis is shown in Fig. 2-(a). The constraint condition for the velocity analysis is shown in Fig. 2-(b). In the velocity analysis, all side boundaries were slid and the top and bottom boundaries were fixed. Young's modulus of material *A* is E_A=210 (GPa) and that of material *B* is E_B=21 (GPa). The interface in the center is optimized under the two volume constraints that the total volume and the volume of layer *A* are constant. The obtained shape is shown in Fig. 3-(a). For comparison with (a), the result obtained under only the total volume constraint is shown in Fig. 3-(b). The portion near the fixed area in the stiffness analysis is more dominated by material *A* with a high Young's modulus in (a) and (b), but the interface shapes obtained are different because of the effect of the volume constraints. Iteration convergence histories of the compliance and the volume for both conditions are shown in Figs. 4-(a) and (b). The values were normalized to those of the initial shape. The compliances of the obtained shapes (a) and (b) are reduced by 44% and 63% from the initial shape, while satisfying each volume constraint, respectively.

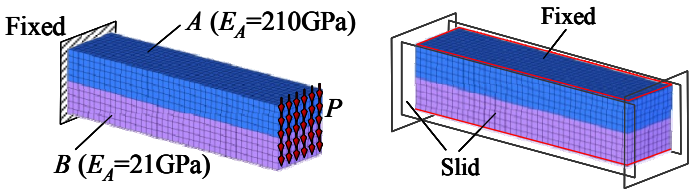

(a) Stiffness analysis (b) Velocity analysis

Figure 2. Initial shape and boundary conditions for problem of cantilever beam with two layers.

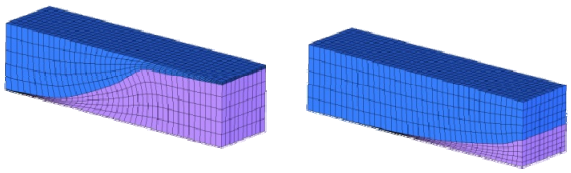

(a) Obtained shape subject to under M_A and M constraints

(b) Obtained shape subject to M constraint

Figure 3. Obtained optimum interfaces of cantilever beam with two layers.

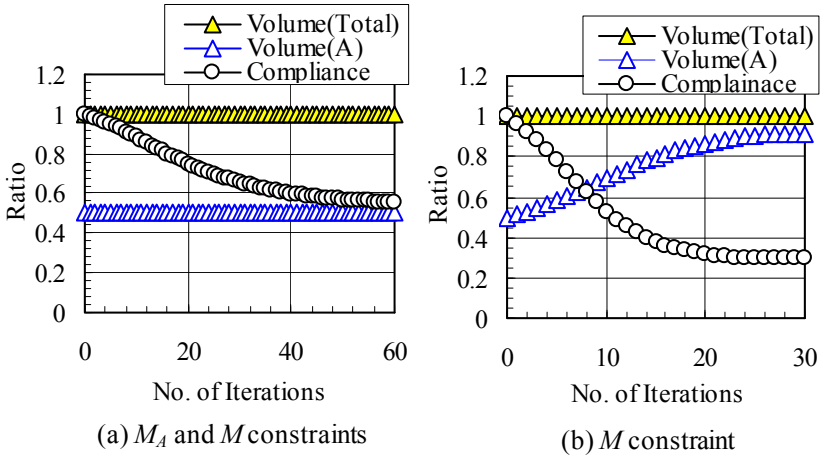

(a) M_A and M constraints (b) M constraint

Figure4. Iteration histories of cantilever beam with two layers

5.2 Cantilever beam problem with three layers

The second problem involves the same cantilever as in the first problem, but one with three layers of two different materials *A* and *B* as shown in Fig. 5-(a). The shapes obtained are

shown in Fig. 5-(b) and -(c), respectively. The total volume and that of material A are constrained so that both are kept constant in (b), and only the total volume is kept constant as the constraint in (c). The portion near the fixed area is more dominated by material A, the same as in the first problem, but the interface shapes differ between the two conditions. The compliances of the obtained shapes (b) and (c) were reduced by 43% and 82% from the initial shape, respectively.

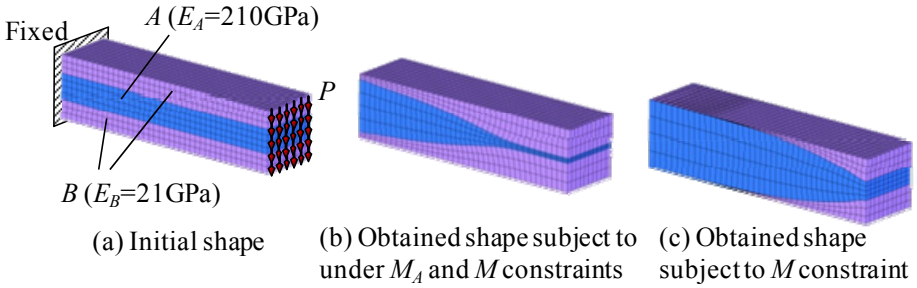

Figure 5: Obtained optimum interfaces of cantilever beam with three layers.

5.3 Both ends clamped beam problem with two layers

The last problem is a both ends clamped beam problem with two different material layers A and B. The initial shape and the boundary condition for the stiffness analysis are shown in Fig. 6-(a). The constraint condition for the velocity analysis is shown in Fig. 6-(b). In the velocity analysis, all side boundaries were slid and the top boundary was fixed. Young's modulus of material A is E_A=21 (GPa) and that of material B is E_B=210 (GPa). The interface in the center and the outer lower boundary are optimized under the two volume constraints that the total volume and the volume of layer A are constant. The obtained shape is shown in Fig. 7-(a). For comparison, the result obtained under the condition that the positions of the materials are reversed is shown in Fig. 7-(b). The interface and lower boundary shapes obtained differ considerably between the two conditions. The compliance reduction for (a) was 57% while that for (b) was 43%.

Conclusion

In this paper, we have proposed a numerical shape optimization method for designing the

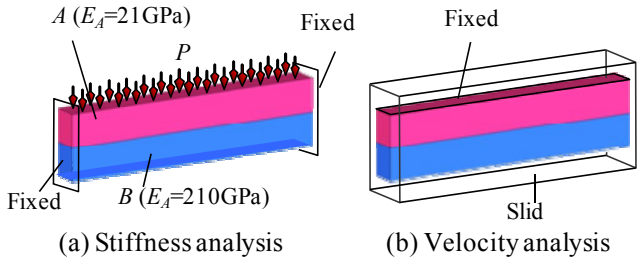

Figure 6. Initial shape and boundary conditions for problem of both ends clamped beam with two layers.

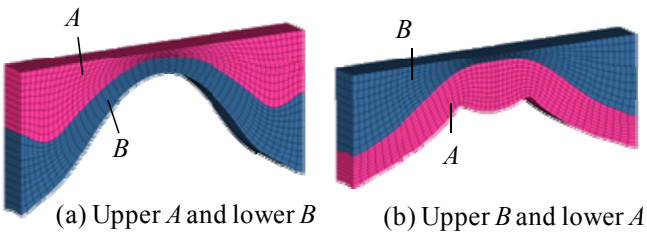

Figure 7. Obtained optimum shapes of both ends clamped beam with two layers.

interface and outer boundary shapes of composite clad structures consisting of two different materials. The compliance was minimized under the volume constraints of the two materials. A distributed-parameter shape optimization problem was formulated and the shape gradient function was derived. Using the traction method, the optimal outer and interface boundary shapes were determined with mesh regularity and without requiring shape design parameterization. Three design examples using this method were presented to demonstrate its effectiveness for designing the optimum interface and outer boundary shapes of composite clad structures consisting of dissimilar materials.

Acknowledgments
This research was supported by grants-in-aid from the Sustainable Mechanical Systems R&D Center at the Toyota Technological Institute.

References
[1] Heinrich, Ch., Duvigneau, R. and Blanchard, L., Isogeometric Shape Optimization in Fluid-Structure Interaction, INRIA-00598367, version 2, (2011).
[2] Lund, E., Moller, H. and Jakobsen, L. A., Shape Desig Optimization of Steady Fluid-Structure Interaction Problems with Large Displacements and Turbulence, Struct Multidisc Optim 25, pp. 383–392 (2003).
[3] Lukas, D. and Kraus, J. K., A Fixed-Grid Finite Element Algebraic Multigrid Approach for Interface Shape Optimization Governed by 2-Dimensional Magnetostatics, in *Large-Scale Scientific Computing,* Springer-Verlag Berlin (2008)
[4] Choi, K. K. and Kim, N. H., *Design Sensitivity Analysis of Structural Systems*, Academic Press, Orland (1986).
[5] Choi, J. H., Lee, B. Y. and Han, J. S., Boundary integral method for shape optimization of interface problems and its application to implant design in dentistry, *Computer Methods in Applied Mechanics and Engineering*, Vol. 190, No. 51, pp. 6909-6926 (2001).
[6] Shimoda, M., Azegami, H. and Sakurai, T., Traction Method Approach to Optimal Shape Design Problems, *SAE Transactions, Journal of Passenger Cars*, 106 (6), pp. 2355-2365 (1998).
[7] Shimoda, M. and Tsuji, J., Non-parametric Shape Optimization Method for Rigidity Design of Automotive Sheet Metal Structures, *SAE Transactions, Journal of Passenger Cars*, SAE Paper 200601-0584 (2006).
[8] Shimoda, M., Iwasa, K. and Azegami, H., A Shape Optimization Method for the Optimal Free-form Design of Shell Structures, *Proceedings of 8th World Congress on Structural and Multidisciplinary Optimization* [CD-ROM], edited by Rodrigues, H. C., Guedes J. M. et al., Lisbon (2009).
[9] Azegami, H., A Solution to Domain Optimization Problems, *Trans. of Jpn. Soc. of Mech. Engs.*, Ser. A, Vol. 60, pp. 1479-1486 (1994) (in Japanese).
[10] Sokolowski, J. and Zolesio, J.P., *Introduction to Shape Optimization*: Shape Sensitivity Analysis, Springer-Verlag, New York, p. 49 (1991).
[11] Azegami, H., Shimoda, M. and Wu, Z. C., Domain Optimization Analysis of Continua, *Computational Mechanics '95*, edited by Atluri, N. Yagawa G. and Cruse, T. A., Vol. 1, Springer, pp. 177-182 (1995).
[12] Azegami, H. and Takeuchi, K., A Smoothing Method for Shape Optimization: Traction Method Using the Robin Condition, *International Journal of Computational Methods*, Vol. 3, No. 1, pp. 21-33 (2006).
[13] Shimoda, M., Motora, S. and Azegami, H., A Practical Solution to Shape Optimization Problem of Solid Structure, *Transactions of the Wessex Institute on the Built Environment*, 106, (Computer Aided Optimum Design of Structures XI, edited by Hernandez V. S. and Brebbia C. A., WIT Press, Southampton, pp. 33-44 (2009).